

Structure and Catalytic Mechanism of LigI: Insight into the Amidohydrolase Enzymes of cog3618 and Lignin Degradation

Merlin Eric Hobbs,[†] Vladimir Malashkevich,[§] Howard J. Williams,[‡] Chengfu Xu,[‡] J. Michael Sander,^{||} Stephen K. Burley,^{||} Steven C. Almo,^{*,§} and Frank M. Raushel^{*,†,‡}

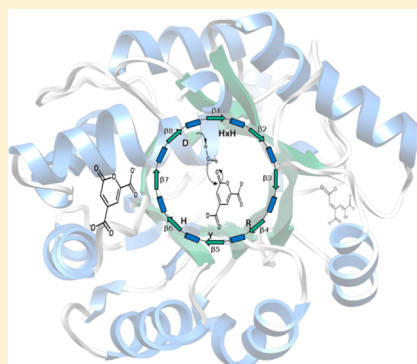
[†]Department of Biochemistry and Biophysics and [‡]Department of Chemistry, Texas A&M University, College Station, Texas 77843, United States

[§]Albert Einstein College of Medicine, 1300 Morris Park Avenue, Bronx, New York 10461, United States

^{||}Lilly Biotechnology Center, 10300 Campus Point Drive, San Diego, California 92121, United States

 Supporting Information

ABSTRACT: LigI from *Sphingomonas paucimobilis* catalyzes the reversible hydrolysis of 2-pyrone-4,6-dicarboxylate (PDC) to 4-oxalomesaconate and 4-carboxy-2-hydroxymuconate in the degradation of lignin. This protein is a member of the amidohydrolase superfamily of enzymes. The protein was expressed in *Escherichia coli* and then purified to homogeneity. The purified recombinant enzyme does not contain bound metal ions, and the addition of metal chelators or divalent metal ions to the assay mixtures does not affect the rate of product formation. This is the first enzyme from the amidohydrolase superfamily that does not require a divalent metal ion for catalytic activity. The kinetic constants for the hydrolysis of PDC are 340 s^{-1} and $9.8 \times 10^6\text{ M}^{-1}\text{ s}^{-1}$ (k_{cat} and k_{cat}/K_m , respectively). The pH dependence on the kinetic constants suggests that a single active site residue must be deprotonated for the hydrolysis of PDC. The site of nucleophilic attack was determined by conducting the hydrolysis of PDC in ^{18}O -labeled water and subsequent ^{13}C nuclear magnetic resonance analysis. The crystal structures of wild-type LigI and the D248A mutant in the presence of the reaction product were determined to a resolution of 1.9 Å. The C-8 and C-11 carboxylate groups of PDC are coordinated within the active site via ion pair interactions with Arg-130 and Arg-124, respectively. The hydrolytic water molecule is activated by the transfer of a proton to Asp-248. The carbonyl group of the lactone substrate is activated by electrostatic interactions with His-180, His-31, and His-33.



Lignin is the most abundant aromatic biomolecule found in nature. This compound and associated degradation products have implications for the production of biofuels and in the manufacture of adhesives and polyesters.¹ The enzyme 2-pyrone-4,6-dicarboxylate lactonase (LigI) plays an important role in the metabolism of lignin-derived aromatic compounds. In the syringate degradation pathway, lignin and tannin-derived compounds containing syringyl moieties are metabolized. Alternatively, lignin-derived compounds containing guaiacyl moieties are metabolized via the protocatechuate 4,5-cleavage pathway.² LigI catalyzes the reversible hydrolysis of 2-pyrone-4,6-dicarboxylate (PDC) to a mixture of 4-carboxy-2-hydroxymuconate (CHM) and 4-oxalomesaconate (OMA) as shown in Scheme 1.^{2,3} Amino acid sequence alignments have identified LigI from *Sphingomonas paucimobilis* as a member of the amidohydrolase superfamily (AHS).

The amidohydrolase superfamily was first identified by Sander and Holm from recognition of the structural and sequence similarities of urease, phosphotriesterase, and adenosine deaminase.⁴ Since the discovery of the AHS, more than 23000 proteins have been classified as members of this superfamily. Members of this superfamily catalyze a diverse set of chemical reactions, including the hydrolysis of amide or ester bonds, deamination of nucleic acids, decarboxylation, isomer-

ization, and hydration.⁵ Proteins in the AHS possess a distorted $(\beta/\alpha)_8$ -TIM barrel structural fold that typically houses an active site containing one to three divalent metal ions. The active site metal ions are ligated to the protein through interactions with residues that originate from the C-terminal ends of β -strands that form the core of the β -barrel. The mononuclear metal centers are formed through ligation with a pair of histidine residues in an HxH motif from β -strand 1, a histidine from β -strand 5, and an aspartate from β -strand 8. Proteins with binuclear metal centers coordinate two divalent cations through ligation with the HxH motif from β -strand 1, a carboxylated lysine (or glutamate) from β -strand 3 or 4, two histidine residues from the ends of β -strands 5 and 6, and an aspartate from β -strand 8. The carboxylated lysine functions as a bridge between the two divalent cations.

In contrast, LigI does not appear to be a metalloenzyme. There is no obvious residue that could bridge a binuclear metal center at the C-terminus of β -strand 3 or 4. In addition, the conserved histidine found at the C-terminal end of β -strand 5 in

Received: March 3, 2012

Revised: April 3, 2012

Published: April 4, 2012



Scheme 1

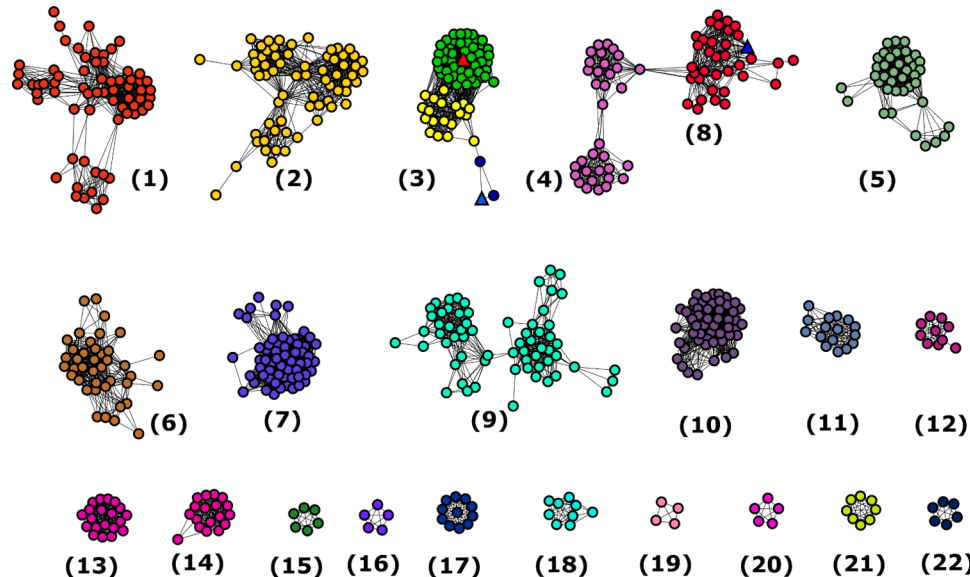
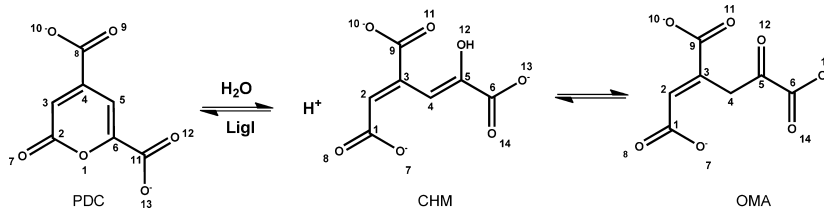


Figure 1. Cytoscape-generated sequence similarity network of cog3618 at a BLAST *E* value cutoff of 10^{-70} . Nodes represent proteins within cog3618 connected to other proteins with an *E* value cutoff of $<10^{-70}$ by lines. The stringency value of 10^{-70} was arbitrarily chosen on the basis of what appears to be the presence of smaller isofunctional groups. The triangle-shaped nodes colored red and blue in group 3 represent LigI from *S. paucimobilis* and 4-SML from *Agrobacterium tumefaciens*, respectively. Circular nodes colored green in group 3 are annotated here as LigI, based on conservation of active site residues of LigI from *S. paucimobilis*. Nodes colored blue in group 3 are predicted to be 4-SML enzymes. The yellow nodes in group 3 are unannotated. The triangle-shaped node colored blue in group 8 is L-rhamnono-1,4-lactonase from *Azotobacter vinelandii*. The rest of the proteins are of unknown function.

nearly all members of the AHS is replaced with a tyrosine in LigI.⁵ These observations suggest that LigI will have an active site that is significantly different from those of the structurally characterized members of the amidohydrolase superfamily.

The AHS has been divided into 24 clusters of orthologous groups (COG) by the National Center for Biotechnology Information (NCBI).⁶ LigI is one of three partially characterized enzymes within cog3618, along with 4-sulfomuconolactonase (4-SML) and L-rhamnono-1,4-lactonase.^{7,8} All three of these enzymes catalyze the hydrolytic cleavage of lactones. A sequence similarity network for cog3618 is presented in Figure 1.^{9,10} The experimentally verified examples of LigI and 4-SML are found in group 3 of cog3618; these two proteins share ~38% sequence identity. The L-rhamnono-1,4-lactonase is found in group 8 of cog3618 and shares ~20% sequence identity with LigI.

Relatively little is known about the mechanism of action of LigI.^{2,11} Previously determined values of k_{cat} for the forward and reverse reactions vary from 110 to 270 s⁻¹. The K_m for PDC hydrolysis is $\sim 70 \mu\text{M}$, and the Michaelis constant for CHM and OMA during lactone synthesis is $\sim 35 \mu\text{M}$. Previous published reports suggested that the addition of divalent metal ions to the assays provides no rate enhancement or is inhibitory.¹¹ Here, we report the crystal structure of LigI in the presence and absence of the product bound in the active site. The catalytic

mechanism for the hydrolysis of PDC was elucidated using pH-rate profiles and active site-directed mutants.

MATERIALS AND METHODS

Materials. All chemicals and buffers were purchased from Sigma Aldrich unless otherwise specified. The synthesis of 2-pyrone-4,6-dicarboxylate was conducted according to published procedures.² All buffers, except for Tris-HCl, were titrated to the stated pH with NaOH.

Expression and Purification of LigI from *S. paucimobilis*. The gene for *S. paucimobilis* LigI (NYSGXRC-10053d, UniProt entry O87170) was synthesized by back translation and codon optimization for *Escherichia coli* expression (Codon Devices, Inc.). The gene was cloned into a custom TOPO-isomerase vector, pSGX3(BC), supplied by Invitrogen. The forward primer was ACCAATGATGAACGTATTCTGAGC, and the reverse primer was CCATTTCCCTCGCTCCAATA-CAATC. The clone encoded Met-Ser-Leu followed by the polymerase chain reaction (PCR) product and Glu-Gly-His₆. Miniprep DNA was transformed into BL21(DE3)-Codon+RIL expression cells (Stratagene), expressed, and made into a 30% glycerol stock for large-scale fermentation.

The expression clones were cultured using High Yield selenomethionine (SeMet) medium (Orion Enterprises, Inc., Northbrook, IL); 50 mL overnight cultures in 250 mL baffled

Table 1. Data Collection and Refinement Statistics for the LigI Crystal Structures^a

	LigI	D248A	D248A	D248N
Protein Data Bank entry	native, pH 8.5 4D8L	substrate, pH 8.5 4DI8	substrate, pH 6.5 4DI9	substrate, pH 4.6 4DIA
wavelength (Å)	0.979	1.075	0.979	1.075
space group	P2 ₁ 2 ₁ 2 ₁	P2 ₁	C2	P2 ₁ 2 ₁ 2 ₁
unit cell dimensions	<i>a</i> = 52.10 Å <i>b</i> = 73.17 Å <i>c</i> = 82.75 Å $\alpha = \beta = \gamma = 90^\circ$	<i>a</i> = 74.35 Å <i>b</i> = 52.13 Å <i>c</i> = 76.54 Å $\alpha = \gamma = 90^\circ$ $\beta = 93.7^\circ$	<i>a</i> = 73.55 Å <i>b</i> = 50.95 Å <i>c</i> = 73.35 Å $\alpha = \gamma = 90^\circ$ $\beta = 91.9^\circ$	<i>a</i> = 52.27 Å <i>b</i> = 54.06 Å <i>c</i> = 96.52 Å $\alpha = \beta = \gamma = 90^\circ$
resolution range (Å)	2.0–20.0	1.8–20.0	1.35–20.0	2.0–20.0
no. of observed reflections	61399	193893	192591	138757
no. of unique reflections	35073	53622	56051	20448
completeness (%)	84.2 (61.8) ^b	99.8 (98.7) ^b	90.6 (46.6) ^b	98.1 (99.9) ^b
<i>I</i> / <i>σI</i>	11.3 (3.5) ^b	18.2 (3.1) ^b	11.7 (3.5) ^b	9.2 (3.0) ^b
<i>R</i> _{merge} (<i>I</i>) ^c	0.057 (0.273) ^b	0.073 (0.332) ^b	0.057 (0.554) ^b	0.080 (0.581) ^b
Refinement				
<i>R</i> _{cryst} (%) ^d	0.174	0.157	0.161	0.181
<i>R</i> _{free} (%) ^d	0.229	0.187	0.183	0.225
no. of protein non-hydrogen atoms	2316	4706	2339	2262
no. of water molecules	235	646	425	123
average <i>B</i> factor (Å ²)	33.7	17.2	16.0	34.5
root-mean-square deviation from the ideal value				
bonds (Å)	0.028	0.010	0.008	0.010
angles (deg)	2.38	1.23	1.28	1.23
torsion angles (deg)	20.1	13.1	13.8	15.1

^aNo σ cutoff was applied; 5% of the reflections were excluded from the refinement and used to calculate *R*_{free}. ^bValues in parentheses indicate statistics for the high-resolution bin. ^c $R_{\text{merge}} = \sum \sum_j |I_j(hkl) - \langle I(hkl) \rangle| / \sum \sum_j |\langle I(hkl) \rangle|$, where *I*_j is the intensity measurement for reflection *j* and $\langle I \rangle$ is the mean intensity over *j* reflections. ^d R_{cryst} or $R_{\text{free}} = \sum ||F_o(hkl)| - |F_c(hkl)||| / \sum |F_o(hkl)|$, where *F*_o and *F*_c are the observed and calculated structure factors, respectively.

flasks were grown at 37 °C from a frozen glycerol stock for 16 h. Overnight cultures were transferred to 2 L baffled shake flasks containing 1 L of HY-SeMet medium (100 µg/mL kanamycin and 30 µg/mL chloramphenicol) and grown to an OD₆₀₀ of ~1.0. SeMet was added for labeling at 90 mg/L, followed by addition of IPTG to a final concentration of 0.4 mM. Cells were further grown at 22 °C for 21 h, harvested using standard centrifugation for 10 min at 39000g, and frozen at –80 °C. Non-SeMet-labeled protein was expressed in ZYP autoinduction medium.¹²

Cells were lysed in 20 mM Tris-HCl (pH 8.0), 0.5 M NaCl, 25 mM imidazole, and 0.1% Tween 20 by sonication. The cellular debris was removed by centrifugation for 30 min (39800g). The supernatant solution was collected and incubated with 10 mL of a 50% slurry of Ni-NTA agarose (Qiagen) for 30 min with gentle stirring. The sample was then poured into a drip column and washed with 50 mL of wash buffer [20 mM Tris-HCl (pH 8.0), 500 mM NaCl, 10% glycerol, and 25 mM imidazole] to remove unbound proteins. The protein of interest was eluted using 25 mL of elution buffer (wash buffer with 500 mM imidazole). Protein-containing fractions were pooled and further purified by gel filtration chromatography with a GE Healthcare HiLoad 16/60 Superdex 200 prep grade column pre-equilibrated with gel filtration buffer [10 mM HEPES (pH 7.5), 150 mM NaCl, 10% glycerol, and 5 mM DTT]. Fractions containing the protein of interest were combined and concentrated by centrifugation in an Amicon Ultra-15 centrifugal filter unit. The final yield and concentration were 62 mg of protein per liter of medium and

8.6 mg/mL, respectively. Electrospray mass spectroscopy (ESI-MS) was used to obtain an accurate mass of the purified protein and confirm selenomethionine labeling (34372 Da with 11 SeMet residues and no N-terminal methionine). The native, unlabeled protein had a molecular mass of 33858 Da (lacking the N-terminal methionine). The expression plasmid is available through the PSI Material Repository as SpCD00298136 (NYSGXRC clone 10053d1BCt7p1). Associated experimental information, including the DNA sequence, is available in the Protein Expression Purification Crystallization Database (<http://sbkb.org/tt>) as TargetID NYSGXRC-10053d.

Construction of Mutant Enzymes. All single-site mutants of LigI were prepared according to the recommendations of the QuikChange PCR procedure manual. Protein expression and purification procedures were performed with slight modifications as described above for wild-type LigI.

Crystallization and Structure Determination. The concentrations of wild-type LigI, D248A, and D248N for crystallization were 17, 15, and 10 mg/mL, respectively, in 20 mM HEPES (pH 7.5). The substrate, PDC, was added to a concentration of 1.0 mM to each mutant protein prior to crystallization. Diffraction quality crystals were grown using the sitting drop vapor diffusion method by mixing 1 µL of protein and 1 µL of reservoir solution and equilibrating the samples against the corresponding reservoir solution. The compositions of the reservoir solutions were as follows: 30% PEG 4000, 0.1 M Tris-HCl (pH 8.5), and 0.2 magnesium chloride for wild-type LigI; 30% PEG 4000, 0.1 M Tris-HCl (pH 8.5), and 0.2 M

sodium acetate or 25% PEG 3350, 0.1 M Bis-Tris (pH 6.5), and 0.2 M sodium chloride for D248A; 30% PEG 4000, 0.1 M sodium acetate (pH 4.6), and 0.2 M ammonium acetate for D248N.

X-ray Data Collection and Crystallographic Refinement. Crystals of LigI with overall dimensions of 0.15 mm × 0.15 mm × 0.15 mm were mounted in cryo-loops directly from the crystallization droplet and flash-cooled in liquid nitrogen. For D248A (pH 6.5), 20% glycerol was added as a cryoprotectant to the droplets before they were frozen. Diffraction data were collected on a Quantum 315 CCD detector (Area Detector Systems Corp., Poway, CA) with 1.075 or 0.979 Å wavelength radiation on beamline X29A (National Synchrotron Light Source, Brookhaven National Laboratory, Upton, NY). Intensities were integrated using HKL2000 and reduced to amplitudes using TRUNCATE (see Table 1).^{13,14} The structure of native LigI was determined using the SeMet SAD method with SHELX^{15,16} and wARP.¹⁷ The structures of the mutant proteins were determined by the molecular replacement method with PHASER.¹⁸ Model building and refinement were performed with COOT and REFMAC.^{14,19} The quality of the final structures was verified with composite omit maps, and stereochemistry was checked with WHAT-CHECK²⁰ and PROCHEK.²¹ LSQKAB and SSM algorithms were used for structural superpositions.^{14,22} Structural figures were prepared using UCSF Chimera.²³

Enzymatic Synthesis of 4-Oxalomesaconate. OMA was synthesized enzymatically from PDC using LigI as a catalyst. The reaction was conducted in 50 mM CHES (pH 10) with 6.0 mM PDC and 10 μM LigI in a volume of 5.0 mL. The reaction was monitored spectrophotometrically at 312 nm until the reaction was complete. The enzyme was removed when the mixture was passed through a VWR centrifugal filter with a molecular mass cutoff of 3 kDa.

Measurement of Lactonase Activity. The forward and reverse reactions catalyzed by LigI were followed spectrophotometrically with a SpectraMax-340 UV-visible spectrophotometer using a differential extinction coefficient ($\Delta\varepsilon_{312}$) of 6248 M⁻¹ cm⁻¹ at 312 nm.^{2,3} Standard assay conditions for the hydrolysis of PDC included 50 mM BICINE (pH 8.25), varying concentrations of PDC (0–300 μM), and LigI in a final volume of 250 μL at 30 °C. For the reverse reaction, standard assay conditions included 50 mM HEPES (pH 7.5), variable concentrations of OMA (0–300 μM), and LigI in a final volume of 250 μL at 30 °C. The kinetic constants were calculated from a fit of the initial velocity data to eq 1 using the nonlinear least-squares fitting program in SigmaPlot 9.0

$$v/E_t = k_{\text{cat}}[A]/(K_m + [A]) \quad (1)$$

where v is the initial velocity, E_t is the total enzyme concentration, k_{cat} is the turnover number, $[A]$ is the substrate concentration, and K_m is the Michaelis constant. The apparent inhibition constants were determined from a fit of the data to eq 2.

$$v/E_t = (k_{\text{cat}}[A])/[K_a(1/K_i) + [A]] \quad (2)$$

Measurement of the Equilibrium Constant. The equilibrium constant for the reaction catalyzed by LigI was measured over the pH range of 6.0–9.5 at 0.25 pH unit intervals using MES (pH 6.0–6.75), HEPES (pH 7.0–8.0), BICINE (pH 8.2–9.0), and CHES (pH 9.0–9.5) to control the pH. In these measurements, LigI was incubated with 250 μM PDC in a final volume of 250 μL until the reaction reached

equilibrium. The fractional concentrations of OMA and PDC at each pH were determined from the absorbance at 312 nm using a differential extinction coefficient of 6248 M⁻¹ cm⁻¹. The equilibrium constant was calculated from a fit of the data to eq 3, where y equals the mole fraction of PDC at equilibrium.

$$y = 1 + [H^+]/K_{\text{eq}} \quad (3)$$

pH-Rate Profiles. The pH dependence of the kinetic constants, k_{cat} and k_{cat}/K_m , was measured over the pH range of 6.5–9.75 at 0.25 pH unit intervals. The buffers used for the pH-rate profiles were MES (pH 6.0–6.75), HEPES (pH 7.0–8.0), BICINE (pH 8.25–9.0), and CHES (pH 9.0–9.75). The final pH values were recorded after the completion of the assay. The profiles for the pH dependence of k_{cat} and k_{cat}/K_m for lactone hydrolysis and synthesis were fit to eqs 4 and 5, respectively

$$\log y = \log[c/(1 + [H^+]/K_a)] \quad (4)$$

$$\log y = \log[c/(1 + K_b/[H^+])] \quad (5)$$

where c is the maximal value for either k_{cat} or k_{cat}/K_m and K_a and K_b are the ionization constants for the groups that must be unprotonated and protonated for catalytic activity, respectively.

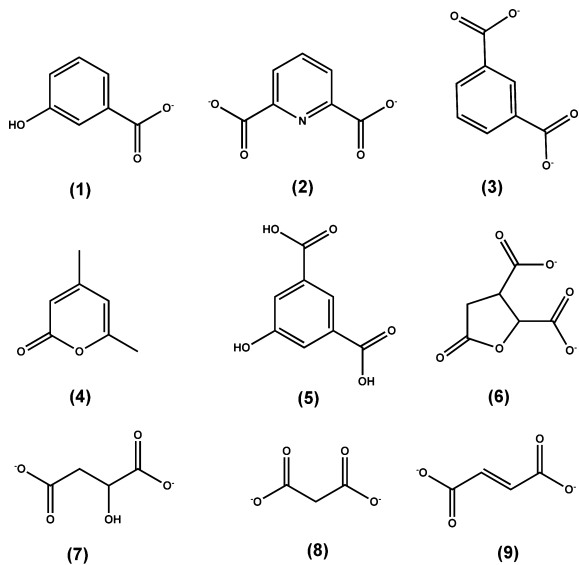
Metal Analysis. The metal content of LigI, substrates, and buffers was determined with an Elan DRC II ICP-MS instrument as previously described.²⁴ Protein samples for ICP-MS analysis were digested with HNO₃ and then refluxed for 30 min.²⁵ All buffers were passed through a column of Chelex 100 (Bio-Rad) to remove trace metal contamination. EDTA, 1,1-phenanthroline, dipicolinic acid, or 2,2'-bipyridine (1.0 mM) was incubated with 1.0 μM LigI in 50 mM buffer at pH values ranging from 6 to 10 to remove divalent metal ions from LigI. The buffers for these experiments included CHES (pH 6.0), HEPES (pH 7.0), BICINE (pH 8.0), and CHES (pH 9.0 and 10.0). The effect of added divalent cations (as the chloride salts) on the catalytic activity of LigI was determined by adding Mn²⁺, Zn²⁺, Co²⁺, Cu²⁺, or Ni²⁺ (0–500 μM) directly to the assay mixtures. LigI (1.0 μM) was also incubated with 50–500 molar equiv of these divalent cations for 24 h at 4 °C in 50 mM HEPES (pH 7.5) and then assayed for catalytic activity.

NMR Analysis of OMA and CHM. The tautomeric distribution of OMA and CHM in solution was determined as a function of pH using heteronuclear multiple-bond correlation (HMBC) NMR spectroscopy with a Bruker Avance III 500 MHz spectrometer with an H-C-N cryoprobe using WATERGATE solvent suppression.

Hydrolysis of PDC in H₂¹⁸O. The site of the hydrolysis of PDC by LigI was determined using NMR spectroscopy in ¹⁸O-labeled water. The reaction was conducted in 100 mM carbonate (pH 9.9) with 10 mM PDC using 10 μM LigI in a final volume of 1.0 mL for 1 h in 50% H₂¹⁸O. At the conclusion of the reaction, LigI was removed from the reaction mixture using a 3 kDa cutoff VWR centrifugal filter. D₂O was added, and the ¹³C NMR spectrum of the product was obtained.

Identification of Inhibitors. Selected compounds (Scheme 2) were evaluated as potential inhibitors of LigI on the basis of structural similarities to PDC, OMA, or CHM. The inhibition assays contained 100 μM PDC, varying concentrations of inhibitor (0–500 μM), 50 mM BICINE (pH 8.25), and LigI in a final volume of 250 μL at 30 °C.

Scheme 2



Sequence Similarity Networks. All protein sequences available through NCBI that are designated as belonging to cog3618 were obtained by a simple search using the query “cog3618”. Protein sequences were then subjected to an all-by-all BLAST using the NCBI stand-alone BLAST program at specific stringency *E* values (10^{-10} , 10^{-20} , 10^{-30} , 10^{-40} , 10^{-50} , 10^{-60} , and 10^{-70}). At a stringency value of 10^{-70} , many of the groups clustered into smaller (and perhaps isofunctional) groups that were given an arbitrary identifying number.

RESULTS

Purification and Properties of LigI from *S. paucimobilis*. 2-Pyrone-4,6-dicarboxylic acid lactonase from *S. paucimobilis* was cloned, expressed in *E. coli*, and purified to homogeneity. The purified LigI did not contain significant amounts of zinc, manganese, iron, copper, cobalt, or nickel (<0.04 equiv per monomer) when analyzed by ICP-MS. The addition of chelating agents directly to the assay solutions did not affect the rate of PDC hydrolysis. The purified LigI was further incubated with EDTA, 1,10-phenanthroline, dipicolinic acid, and 2,2'-bipyridine at pH values from 6 to 10 in an attempt to remove tightly bound metals, but the addition of these potent chelators did not change the catalytic activity of LigI. The addition of Mn^{2+} , Zn^{2+} , Co^{2+} , Cu^{2+} , or Ni^{2+} directly to the assay solutions had no effect on the catalytic activity of LigI. Therefore, LigI does not appear to require a divalent cation for enzymatic activity.

The change in absorbance when PDC is converted to OMA at pH 10.0 is presented in Figure 2. There is an absorption maximum for PDC at 312 nm that is lost upon conversion to OMA. The kinetic constants for the hydrolysis of PDC to OMA and CHM were determined at pH 8.25 to be $342 \pm 25 s^{-1}$, $48 \pm 11 \mu M$, and $(7.5 \pm 1.0) \times 10^6 M^{-1} s^{-1}$ (k_{cat} , K_m , and k_{cat}/K_m , respectively). The kinetic constants in the reverse reaction for the synthesis of PDC from OMA and CHM at pH 8.25 were $116 \pm 6 s^{-1}$, $18 \pm 4 \mu M$, and $(4.9 \pm 0.7) \times 10^6 M^{-1} s^{-1}$ (k_{cat} , K_m , and k_{cat}/K_m , respectively).

NMR Spectra for OMA and CHM. The product of the enzymatic reaction existed in two forms depending on the pH. At pH 10, the keto form (OMA) was predominant as shown by the presence of singlet peaks at δ 6.58 (1 H, H-2) and δ 3.92 (2

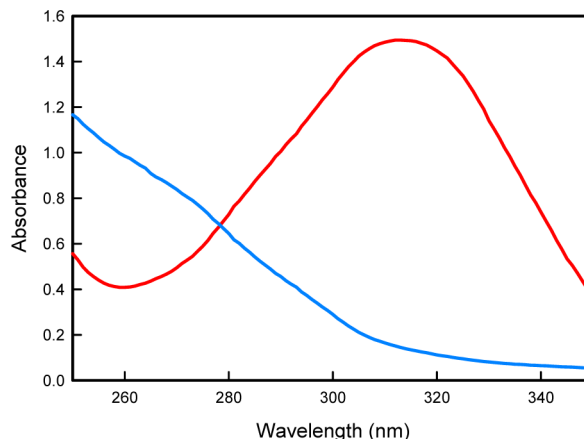


Figure 2. UV-visible absorbance spectrum of 0.3 mM PDC (red) and the hydrolysis product after the addition of LigI (blue) at pH 10. The maximal absorbance change is at 312 nm with a differential extinction coefficient, $\Delta\epsilon$, of $6248 M^{-1} cm^{-1}$.

H, H-2) in the proton NMR spectrum. The carbon spectrum showed peaks for carbonyl carbons at δ 202.0 (C-5), 175.1 (C-1), 175.0 (C-6), and 168.6 (C-9), vinyl carbons at δ 136.9 and 132.8, and an aliphatic carbon at δ 39.8 (C-4). A DEPT experiment indicated that the carbon at δ 132.8 had a single proton attached (C-2), while the carbon producing the peak at δ 39.8 had two attached protons (C-4). The vinyl carbon peak at δ 136.9 is therefore due to C-3. An HMBC experiment showed long-range couplings from the proton peak at δ 3.92 to the two vinyl carbons and carbonyl carbons at δ 202.0 and 175.0. The proton peak at δ 6.58 showed cross-peaks to the carbonyl carbon at δ 175.0, the vinyl carbon at δ 136.9, and the aliphatic carbon at δ 39.8. These data indicated that the peak at δ 175.0 correlating to both proton peaks was C-9. Because of chemical shift considerations, the peak at δ 168.6 is due to C-6, indicating that the peak at δ 175.1 comes from C-1.

At pH 6, the enol form (CHM) was predominant. Its proton spectrum consisted of two doublets at δ 7.19 (H-2) and δ 6.70 (H-4) with a coupling constant of 1.3 Hz. The carbon spectrum showed carbonyl carbon peaks at δ 170.4, 165.5, and 165.4 and vinyl peaks at δ 153.9, 152.7, 116.4, and 108.1. A DEPT experiment indicated the carbons at δ 116.4 and 108.1 each had a single attached proton. An HSQC experiment showed that the proton at δ 7.19 was attached to the carbon at δ 116.4 (C-2), and the proton at δ 6.70 was attached to the carbon at δ 108.1 (C-4). The HMBC experiment indicated the proton at δ 7.19 had long-range couplings to the carbonyl carbons at δ 170.4 (C-1) and δ 165.4 (C-6) and a vinyl carbon at δ 153.9 (C-3). The peak at δ 6.70 correlated to the carbonyl at δ 165.5 (C-6) and a vinyl carbon at δ 152.7 (C-5). The relative amounts of the two forms at given pH values as estimated by protonated vinyl carbon peak heights were 100% OMA and 0% CHM (pH 10), 90% OMA and 10% CHM (pH 9), 55% OMA and 45% CHM (pH 8), 5% OMA and 95% CHM (pH 7), and 2% OMA and 98% CHM (pH 6).

Hydrolysis of PDC in $H_2^{18}O$. The regiochemistry for the attack of water on PDC has not previously been determined. Water could attack C-2 with cleavage of the C-2–O-1 bond. Alternatively, water could attack C-6 with cleavage of the C-6–O-1 bond. The enzymatic reaction was conducted in 50% $H_2^{18}O$ to determine the electrophilic center of PDC that reacts with water. If water attacks C-2, then the C-1 carboxylate group of OMA will be labeled with ^{18}O , whereas if the attack occurs

C-6, then the C-5 carbonyl group of OMA will be labeled. Shown in Figure 3A is the ^{13}C NMR spectrum of the C-1

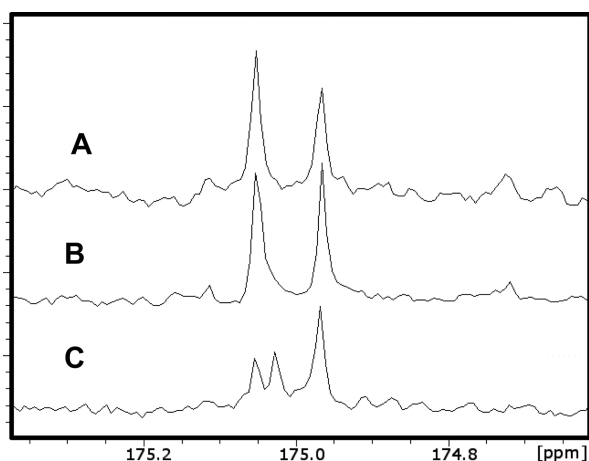


Figure 3. (A) NMR spectrum of OMA in water at pH 9.0. (B) NMR spectrum of OMA incubated in 50% H_2^{18}O at pH 9.0. (C) NMR spectrum of OMA produced enzymatically from PDC in H_2^{18}O at pH 9.0.

carboxylate of the product when the enzymatic reaction was conducted in unlabeled water at pH 9.9. The C-1 carboxylate of OMA appears at δ 175.04 and is a single resonance that is adjacent to the resonance for the C-9 carboxylate at δ 174.96. When the reaction was conducted in H_2^{18}O , the C-1 carboxylate of OMA appears as two distinct resonances with a separation of ~ 0.03 ppm, reflecting the small chemical shift difference for OMA with a single ^{18}O label (Figure 3C). There was no change in the resonance for the C-1 carboxylate when H_2^{18}O was added to OMA after removal of the enzyme (Figure 3B). Therefore, under the conditions of these experiments, the attack by water/hydroxide occurs directly at C-2 of PDC.

pH-Independent Equilibrium Constant. The reaction catalyzed by LigI is reversible, and the equilibrium concentrations of PDC and OMA/CHM are dependent on the solution pH. The equilibrium constant for this reaction was determined by allowing the hydrolysis reaction to reach completion at pH values ranging from 6 to 10. The concentration of PDC was determined from the change in absorbance at 312 nm, and the results are presented in Figure 4. The equilibrium constant, from a fit of the data to eq 2, was determined to be $5.7 \times 10^{-9} \text{ M}^{-1}$. At pH 8.25, the relative concentrations of PDC and the hydrolysis products are thus equal to one another. The Haldane relationship for this reaction at this pH value is presented in eq 6. Substitution of the k_{cat}/K_m values for the substrate and product determined at pH 8.25 gives an apparent equilibrium constant of 1.5, which is reasonably close to the experimentally determined value of 1.0.

$$K_{\text{eq}} = [\text{OMA}_{\text{eq}}]/[\text{PDC}_{\text{eq}}] = (k_{\text{cat}}/K_{\text{PDC}})/(k_{\text{cat}}/K_{\text{OMA}}) \quad (6)$$

Identification of Inhibitors. Nine compounds (see Scheme 2) were tested as potential inhibitors of LigI as a probe of the structural requirements for ligand binding. Of the compounds tested, only pyridine-2,4-dicarboxylic acid (**2**) and 5-hydroxyisophthalic acid (**5**) inhibited the hydrolysis of PDC. The apparent inhibition constants for pyridine-2,4-dicarboxylic acid and 5-hydroxyisophthalic acid are 75 ± 2 and $40 \pm 3 \mu\text{M}$, respectively, from fits of the data to eq 2.

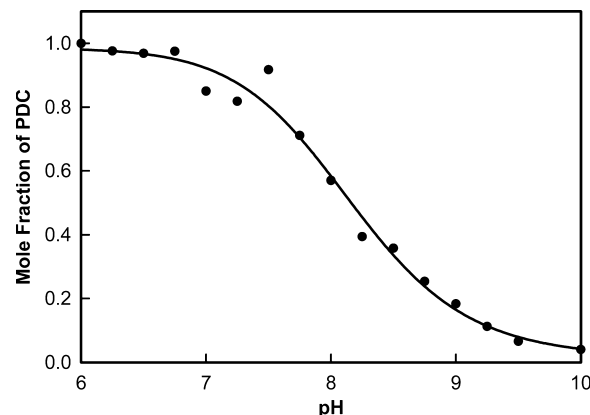


Figure 4. Effect of pH on the equilibrium concentrations of PDC and OMA/CHM. The line represents a fit of the data to eq 3. The equilibrium constant for the reaction illustrated in Scheme 1 is $5.7 \times 10^{-9} \text{ M}^{-1}$.

pH-Rate Profiles. Kinetic constants for the hydrolysis and synthesis of PDC by LigI were measured as a function of pH to identify potential active site residues whose involvement in catalysis is dependent on the state of protonation. The profiles for the forward and reverse reactions are presented in Figure 5. The kinetic $\text{p}K_a$ values for the hydrolysis of PDC are 7.5 ± 0.1 for k_{cat} and k_{cat}/K_m . The kinetic $\text{p}K_a$ values for the condensation of OMA are 8.6 ± 0.1 and 7.5 ± 0.1 for k_{cat} and k_{cat}/K_m , respectively.

Structure of Wild-Type LigI. The crystal structure of native LigI was determined by single anomalous dispersion (SAD) at 2.0 Å resolution. The model contains protein residues Leu-3—Glu-296 and 225 water molecules, most of which are well-defined in the electron density map. The protein has a distorted TIM-barrel fold, and the wide opening on one end of the barrel suggests the entrance to the active site (Figure 6A). The closest structural homologue in the Protein Data Bank (PDB) is a putative 2-pyrone-4,6-dicarboxylate lactonase from *Pseudomonas putida* [PDB entry 2FFI, root-mean-square deviation (rmsd) of 2.8 Å] with a level of sequence identity of 31%.

Structure of the D248A Mutant. To reveal the structural details of the interactions of LigI with substrate, the inactive mutant D248A was produced and cocrystallized with the substrate. Diffraction data were collected for the complex at pH 6.5 and 8.5 (Table 1). In both structures, the ligand is well-defined in the corresponding electron density maps. Substrate binding results in closure of the active site and large-scale rearrangement of two loops: Phe-127—Lys-137 and, to a lesser extent, Ser-44—Pro-51 (Figure 6B). As a result of this structural rearrangement, the first loop transforms from an α -helical conformation into a coiled conformation, and the guanidinium group of Arg-130 moves by 6.1 Å to directly contact the substrate C-8 carboxylic group and to close the entrance of the active site. The phenolic side chain of Tyr-49 moves 14.4 Å to be in direct contact with the C-11 carboxylate of PDC.

At pH 8.5, an almost equal mixture of the substrate and product was observed in the active site. The presence of the product can be explained by residual catalytic activity or spontaneous hydrolysis of the substrate in solution. Interestingly, at pH 6.5, only CHM is present in the active site. The electron densities for the bound substrate/product ligands in the active site of LigI at pH 8.5 and 6.5 are shown in panels A

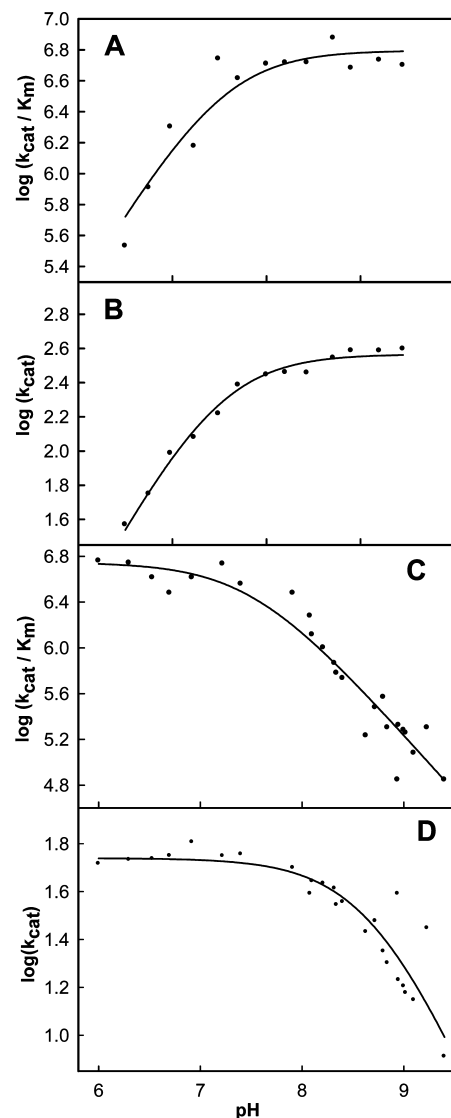


Figure 5. pH–rate profiles for the enzymatic hydrolysis and synthesis of PDC. (A) pH–rate profile for $\log(k_{\text{cat}}/K_m)$ for the hydrolysis of PDC. (B) pH–rate profile for $\log(k_{\text{cat}})$ for the hydrolysis of PDC. The lines for panels A and B represent the fits of the data to eq 4. (C) pH–rate profile for $\log(k_{\text{cat}}/K_m)$ for the synthesis of PDC. (D) pH–rate profile for $\log(k_{\text{cat}})$ for the synthesis of PDC. The lines for panels C and D represent the fit of the data to eq 5.

and B of Figure 7, respectively. PDC forms multiple interactions in the active site: the C-4 carboxylate forms four hydrogen bonds with Arg-130, Asn-253, and Tyr-156; the C-6 carboxylate forms four hydrogen bonds with Arg-124, Tyr-49, and Ser-77; and the C-2 carbonyl group forms four hydrogen bonds with His-31, His-180, and a water molecule. CHM occupies a position similar to that of the substrate and makes multiple interactions: the C-9 carboxylate forms four hydrogen bonds with Arg-130, Asn-253, and Tyr-156; the C-6 carboxylate forms four hydrogen bonds with Arg-124, Tyr-49, and Ser-77; and the remaining carboxylate group (C-1) forms four hydrogen bonds with His-31, His-180, His-33, and a water molecule. The C-5 hydroxyl group of the product forms two hydrogen bonds with Arg-124. Nearby, Arg-217 forms hydrogen bonds with acetate and another water molecule (Figure 8).

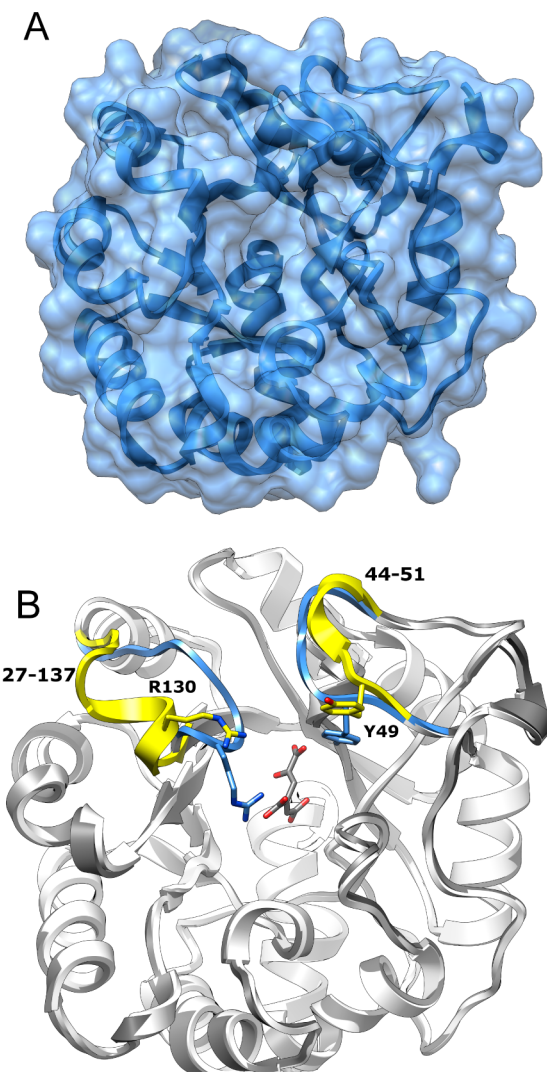


Figure 6. Structure of native LigI and the D248A mutant. (A) Native LigI. The narrow crevice on top of the solvent accessible surface corresponds to the active site entrance. (B) View of CHM-bound D248A LigI (white) superimposed onto the wild-type apo form of LigI (gray). The two loops, Phe-127–Lys-137 and Ser-44–Pro-51, that exhibit a change in conformation upon substrate binding are color-coded as follows: yellow for native LigI (apo) and blue for CHM-bound D248A.

Structure of the D248N Mutant. The structure of the D248N mutant was determined from crystals grown at pH 4.6 in the presence of the purified product PDC. The refined electron density did not show the presence of either substrate or product in the active site. This can be explained by the reduced affinity of the active site for substrate/product under very acidic conditions. The structure of the D248N mutant is very similar to the structure of ligand-free wild-type LigI (rmsd of 0.42 Å), and the conformations of Asn-248 in the mutant enzyme and Asp-248 in the wild-type enzyme are identical.

Mutagenesis of LigI. Residues in LigI that align with the prototypical metal-coordinating residues in the AHS were mutated. These residues included His-31 and His-33 from the C-terminal end of β -strand 1, His-180 from the end of β -strand 6, and Asp-248 from the end of β -strand 8. Additional active site residues that were mutated included Tyr-156, Arg-124, Tyr-49, Arg-130, Arg-217, and Arg-183. Tyr-156 from the end of β -

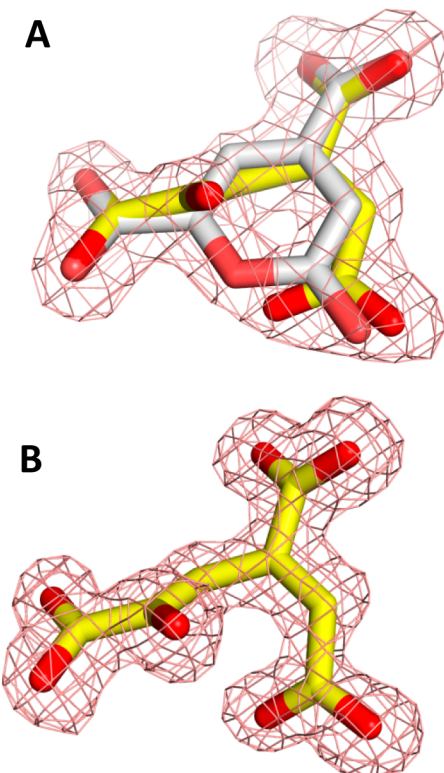


Figure 7. Refined electron density ($2F_o - F_c$ contoured at 1σ) of the ligand in the active site of LigI. (A) Equimolar amounts of substrate (PDC, white) and product (CHM, yellow) at pH 8.5. (B) Product only (CHM, yellow) at pH 6.5.

strand 5 replaces the conserved histidine residue that coordinates a divalent cation in those members of the AHS with either a mononuclear or binuclear metal center. Arg-124 from the end of β -strand 4 is positioned to occupy the space filled by the residue that bridges the two divalent cations in those members of the AHS with a binuclear metal center. Tyr-49, Arg-130, and Arg-183 are in the active site and interact with the substrate/product. The kinetic constants for these mutants are listed in Table 2.

■ DISCUSSION

Potential Role of Divalent Metal Ions. Although all well-characterized amidohydrolases require one to three divalent metal ions for catalytic activity, LigI and other members of cog3618 exhibit active site differences with respect to other amidohydrolase superfamily members that argue they are not metalloenzymes. We were unable to detect bound metal ions via ICP-MS in the samples of recombinant LigI prepared for this investigation. In addition, metal ion chelators had no effect on the catalytic activity of LigI, and the addition of divalent cations to enzymatic assays had no effect on reaction rates. Therefore, we conclude that LigI from *S. paucimobilis* does not require a divalent cation for catalytic activity and does not bind divalent metals to any significant extent. To the best of our knowledge, this work provides the first documented example of an enzyme from the AHS that does not require a divalent cation to bind in the active site for catalytic activity. It will be of mechanistic interest to determine whether other proteins of unknown function within cog3618 require divalent cations for catalytic activity.

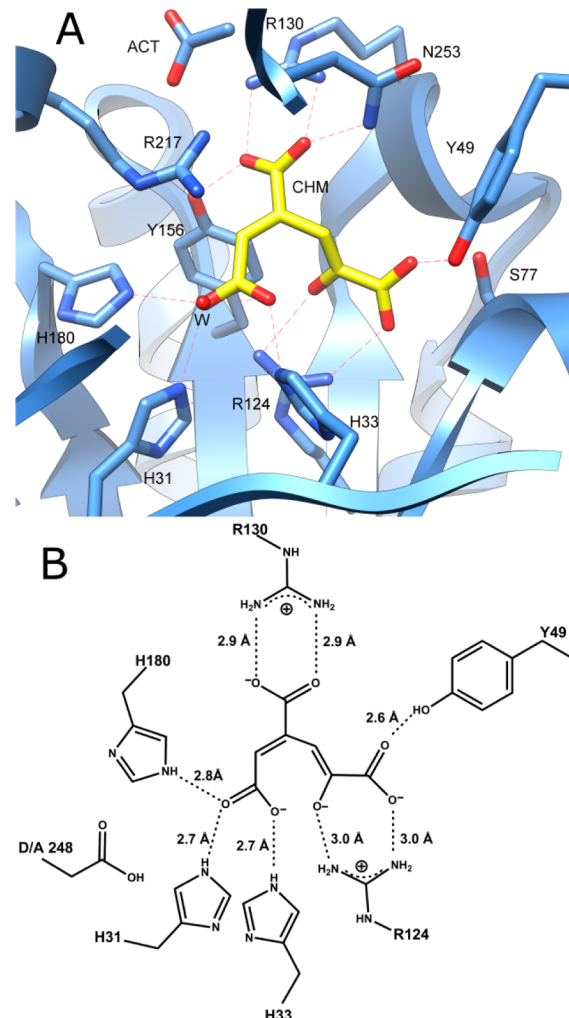


Figure 8. (A) CHM bound in the active site of the D248A mutant of LigI at pH 6.5. No PDC was detected at this pH. (B) Active site structure of D248A with CHM in the active site.

Active Site of LigI. Nearly all members of the AHS have a constellation of five amino acid residues that are conserved within the active site and required for metal ion binding and/or

Table 2. Catalytic Constants for Wild-Type LigI and Its Various Mutants for PDC Hydrolysis^a

enzyme	k_{cat} (s^{-1})	K_m (μM)	k_{cat}/K_m ($M^{-1} s^{-1}$)
wild-type	342 ± 25	48 ± 11	$(7.1 \pm 1) \times 10^6$
D248A	0.0013 ± 0.0001	116 ± 18	$(1.6 \pm 0.2) \times 10$
D248N	0.023 ± 0.001	66 ± 13	$(2.0 \pm 0.34) \times 10^2$
R124M	0.020 ± 0.001	90 ± 15	$(2.0 \pm 0.22) \times 10^2$
R130M	5.0 ± 0.4	465 ± 104	$(1.1 \pm 0.7) \times 10^4$
H31N	0.40 ± 0.04	720 ± 122	$(5.0 \pm 0.37) \times 10^2$
R217M	0.42 ± 0.02	67 ± 10	$(6.3 \pm 0.4) \times 10^3$
H180A	8.0 ± 0.9	214 ± 44	$(3.7 \pm 0.4) \times 10^4$
H180C	32 ± 4	41 ± 7	$(7.8 \pm 0.5) \times 10^5$
H33N	3.6 ± 0.3	89 ± 20	$(4.1 \pm 0.6) \times 10^4$
Y49F	26 ± 2	217 ± 41	$(1.2 \pm 0.02) \times 10^5$
Y156F	8.7 ± 0.3	238 ± 19	$(3.7 \pm 0.02) \times 10^5$
R183M	196 ± 6	64 ± 6	$(3.0 \pm 0.02) \times 10^6$

^aStandard assay conditions for the hydrolysis of PDC included 50 mM BICINE, pH 8.25, and 30 °C.

proton transfers.⁵ These residues include two histidine residues from the end of β -strand 1, two additional histidine residues from the ends of β -strands 5 and 6, and a conserved aspartate residue from the end of β -strand 8. In LigI, the three histidine residues (H31, H33, and H180) from the ends of β -strands 1 and 6 are conserved in addition to the aspartate (D248) from the end of β -strand 8. The histidine from the end of β -strand 5 is absent. Because LigI does not require the binding of divalent cations for the expression of catalytic activity, the functional role of these conserved residues must be different than they are for the rest of the amidohydrolase superfamily.

A structural alignment of the active site of LigI and phosphotriesterase (PTE), an enzyme with a prototypical binuclear metal active site, is presented in Figure 9A. The HxH

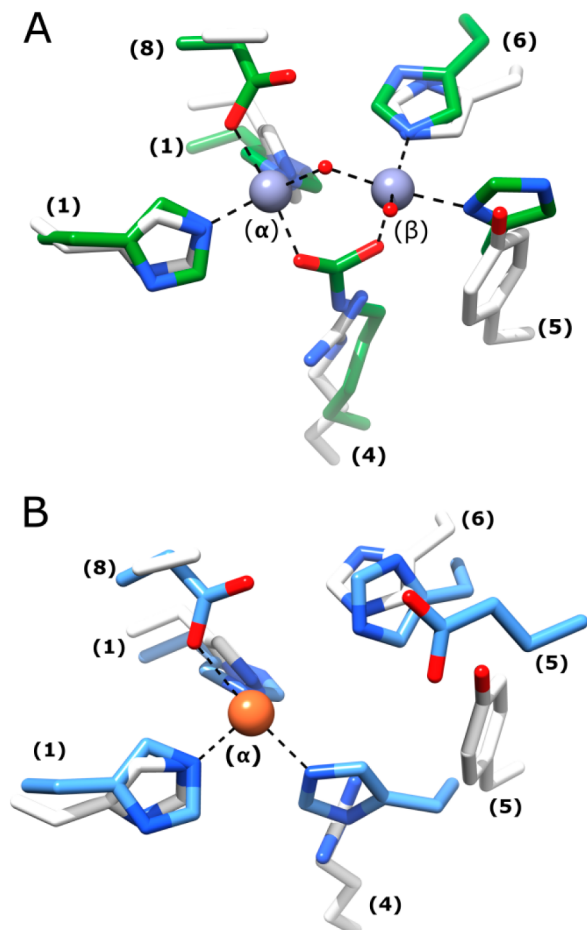


Figure 9. (A) Active site of D248A LigI structurally aligned with the binuclear metal center of phosphotriesterase (PTE). The active site is color-coded as follows: green for PTE (PDB entry 1hzy) and white for the D248A LigI active site. (B) Active site of D248A LigI structurally aligned with the mononuclear metal center found in the active site of cytosine deaminase. The active sites are color-coded as follows: blue for CDA (PDB entry 1k70) and white for the D248A LigI active site. Numbers in parentheses indicate the β -strand origin of each residue.

motif from β -strand 1, the histidine from β -strand 6, and the aspartate from β -strand 8 of LigI align well with the corresponding residues of PTE. In addition, Tyr-156 from β -strand 5 of LigI aligns with the conserved histidine from β -strand 5 of PTE and Arg-124 from β -strand 4 of LigI aligns with the carboxylated lysine from β -strand 4 of PTE. In PTE, the carboxylated lysine serves to bridge the two divalent cations.

The active site of LigI is overlaid with the active site of cytosine deaminase (CDA), a mononuclear metal active site in Figure 9B. The HxH motif from β -strand 1, the histidine from β -strand 6, and the aspartate from β -strand 8 of LigI align reasonably well with the corresponding residues of CDA. However, Tyr-156 from LigI does not align with the conserved histidine from β -strand 5 of CDA. The inability of LigI to bind a divalent metal appears to stem from the presence of the positively charged Arg-124 in the active site.

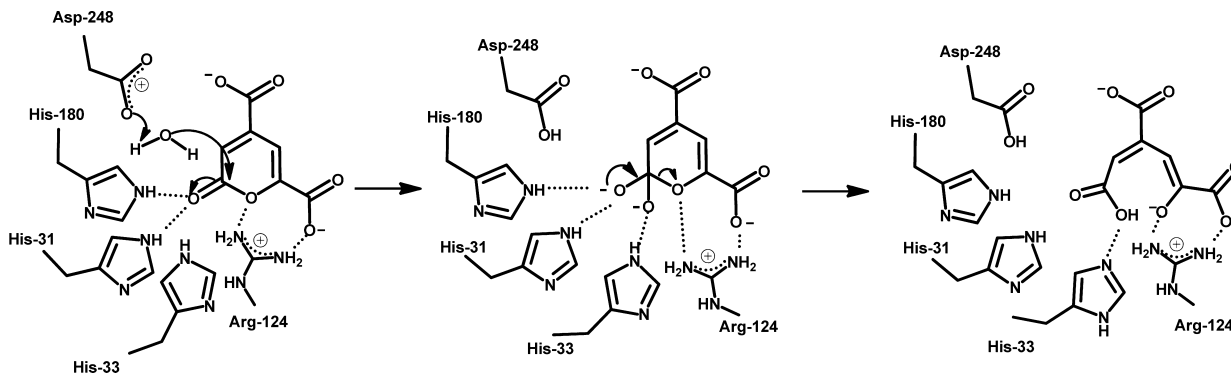
Role of Conserved Residues and Mechanism of Action.

A working model for the hydrolysis of PDC by LigI is presented in Scheme 3. In this mechanism, some of the conserved AHS active site residues, which normally participate in metal coordination, have different catalytic roles in the function of this protein. The four residues in question are His-31, His-33, His-180, and Asp-248. The binding of PDC is facilitated by ion pair interactions between residues Arg-130 and Arg-124 and the C-8 and C-11 carboxylates, respectively. There is an additional electrostatic interaction between Tyr-49 and the C-11 carboxylate. The lactone carbonyl group of the substrate is polarized by electrostatic interactions with the three conserved histidine residues: His-31, His-33, and His-180. Asp-248 is positioned in the active site to deprotonate an active site water molecule for nucleophilic attack on the C-2 carbonyl group of the substrate. The orientation of Asp-248 allows for the attack on the *re* face of PDC, which is consistent with the relative orientation of attack determined previously for other members of the amidohydrolase superfamily.²⁶ After formation of the tetrahedral intermediate, the C-2–O-1 bond is cleaved with support of the electrostatic interaction of the guanidino group of Arg-124.

Further support for the proposed mechanism of action comes from our structure with substrate/product ligands bound to the enzyme and the catalytic properties of selected LigI mutants. The importance of D248 is confirmed by the nearly complete absence of activity for the D248A and D248N mutants. These mutants are reduced in activity by 4–5 orders of magnitude (for either k_{cat} or k_{cat}/K_m). Of the three conserved histidine residues in the active site, the mutation of His-31 results in the greatest loss of catalytic power. Mutation of this residue to asparagine reduces k_{cat}/K_m by more than 4 orders of magnitude. Mutation of either His-33 or His-180 reduces this kinetic constant by approximately 2 orders of magnitude. The mutation of Tyr-49 to phenylalanine reduces k_{cat}/K_m ~60-fold, and mutation of Arg-124 reduces k_{cat}/K_m by a factor of ~30000. The pH–rate profiles are consistent with an active site residue that must be deprotonated for catalytic activity. This residue is most likely assigned to either Asp-248 or His-31. Tyr-156 is 2.5 Å from the C-8 carboxylate oxygen and 3.6 Å from C-2.

Additional LigI Sequences. Candidate LigI sequences were obtained from the NCBI protein database through a BLAST search with LigI from *S. paucimobilis* as the query sequence. The candidate sequences had to meet a minimum *E* value cutoff of 10^{-70} to be considered for further analysis. All protein sequences were aligned with that of the experimentally verified LigI from *S. paucimobilis*. Sequences were considered to be LigI if they conserve the following active site residues: His-31, His-33, Tyr-49, Arg-124, Arg-130, Tyr-156, His-180, and Asp-248. The 66 sequences that conform to the specific conserved residues are now postulated to be LigI proteins and are shown as green nodes in group 3 of Figure 1 and are listed in Table S1 of the Supporting Information.

Scheme 3



ASSOCIATED CONTENT

Supporting Information

A list of bacterial proteins predicted to catalyze the same reaction as LigI (Table S1). This material is available free of charge via the Internet at <http://pubs.acs.org>.

Accession Codes

The X-ray coordinates and structure factors of LigI have been deposited in the Protein Data Bank as entries 4D8L, 4DI8, 4DI9, and 4DIA.

AUTHOR INFORMATION

Corresponding Author

*F.M.R.: telephone, (979) 845-3373; fax, (979) 845-9452; e-mail, raushel@tamu.edu. S.C.A.: telephone, (718) 430-2746; fax, (718) 430-8565; e-mail, almo@aecom.yu.edu.

Funding

This work was supported in part by the National Institutes of Health (GM 71790 and GM 74945) and the Robert A. Welch Foundation (A-840).

Notes

The authors declare no competing financial interest.

ACKNOWLEDGMENTS

We are grateful to Rafael Toro for his help with crystallization and to the staff of beamline X29 for their help with the collection of diffraction data.

REFERENCES

- (1) Hishida, M., Shikinaka, K., Katayama, Y., Kajita, S., Masai, E., Nakamura, M., Otsuka, Y., Ohara, S., and Shigehara, K. (2009) Polyesters of 2-pyrone-4,6-dicarboxylic acid (PDC) as bio-based plastics exhibiting strong adhering properties. *Polym. J.* **41**, 297–302.
- (2) Kersten, P. J., Dagley, S., Whittaker, J. W., Arciero, D. M., and Lipscomb, J. D. (1982) 2-Pyrone-4,6-dicarboxylic acid, a catabolite of gallic acids in *Pseudomonas* species. *J. Bacteriol.* **152**, 1154–1162.
- (3) Maruyama, K. (1983) Purification and properties of 2-pyrone-4,6-dicarboxylate hydrolase. *J. Biochem.* **93**, 557–565.
- (4) Holm, L., and Sander, C. (1997) An Evolutionary Treasure: Unification of a Broad Set of Amidohydrolases Related to Urease. *Proteins: Struct., Funct., Genet.* **28**, 72–82.
- (5) Seibert, C. M., and Raushel, F. M. (2005) Structural and Catalytic Diversity within the Amidohydrolase Superfamily. *Biochemistry* **44**, 6383–6391.
- (6) Tatusov, R. L., Natale, D. A., Garkavtsev, I. V., Tatusova, T. A., Shankavaram, U. T., Rao, B. S., Kiryutin, B., Galperin, M. Y., Fedorova, N. D., and Koonin, E. V. (2001) The COG Database: New Developments in Phylogenetic Classification of Proteins from Complete Genomes. *Nucleic Acids Res.* **29**, 22–28.
- (7) Halak, S., Basta, T., Buerger, S., Contzen, M., Wray, V., Pieper, D. H., and Stoltz, A. (2007) 4-Sulfomuconolactone hydrolases from *Hydrogenophaga intermedia* S1 and *Agrobacterium radiobacter* S2. *J. Bacteriol.* **189**, 6998–7006.
- (8) Watanabe, S., Saimura, M., and Makino, K. (2008) Eukaryotic and bacterial gene clusters related to an alternative pathway of nonphosphorylated L-rhamnose metabolism. *J. Biol. Chem.* **283**, 20372–20382.
- (9) Smoot, M. E., Ono, K., Ruscheinski, J., Wang, P. L., and Ideker, T. (2011) Cytoscape 2.8: New features for data integration and network visualization. *Bioinformatics* **27**, 431–432.
- (10) Atkinson, H. J., Morris, J. H., Ferrin, T. E., and Babbitt, P. C. (2009) Using sequence similarity networks for visualization of relationships across diverse protein superfamilies. *PLoS One* **4**, e4345.
- (11) Masai, E., Shinohara, S., Hara, H., Nishikawa, S., Katayama, Y., and Fukuda, M. (1999) Genetic and Biochemical Characterization of a 2-Pyrone-4,6-dicarboxylic Acid Hydrolase Involved in the Protocatechuic 4,5-Cleavage Pathway of *Sphingomonas paucimobilis* SKY-6. *J. Bacteriol.* **181**, 55–62.
- (12) Studier, F. W. (2005) Protein production by auto-induction in high density shaking cultures. *Protein Expression Purif.* **41**, 207–234.
- (13) Otwinowski, Z. M., and Minor, W. (1997) Processing of X-ray diffraction data collected in oscillation mode. *Methods Enzymol.* **276**, 307–326.
- (14) Collaborative Computational Project Number 4 (1994) The CCP4 Suite: Programs for Protein Crystallography. *Acta Crystallogr. S0*, 760–763.
- (15) Sheldrick, G. M. (2002) Macromolecular phasing with SHELXE. *Z. Kristallogr.* **217**, 644–650.
- (16) Schneider, T. R., and Sheldrick, G. M. (2002) Substructure solution with SHELXD. *Acta Crystallogr.* **58**, 1772–1779.
- (17) Langer, G., Cohen, S. X., Lamzin, V. S., and Perrakis, A. (2008) Automated macromolecular model building for X-ray crystallography using ARP/wARP version 7. *Nat. Protoc.* **3**, 1171–1179.
- (18) Storoni, L. C., McCoy, A. J., and Read, R. J. (2004) Likelihood-enhanced fast rotation functions. *Acta Crystallogr. D60*, 432–438.
- (19) Emsley, P., and Cowtan, K. (2004) Coot: Model-building tools for molecular graphics. *Acta Crystallogr. D60*, 2126–2132.
- (20) Hooft, R. W., Vriend, G., Sander, C., and Abola, E. E. (1996) Errors in protein structures. *Nature* **381**, 272.
- (21) Laskowski, R. A., Moss, D. S., and Thornton, J. M. (1993) Main-chain bond lengths and bond angles in protein structures. *J. Mol. Biol.* **231**, 1049–1067.
- (22) Krissinel, E., and Henrick, K. (2004) Secondary-structure matching (SSM), a new tool for fast protein structure alignment in three dimensions. *Acta Crystallogr. D60*, 2256–2268.
- (23) Pettersen, E. F., Goddard, T. D., Huang, C. C., Couch, G. S., Greenblatt, D. M., Meng, E. C., and Ferrin, T. E. (2004) UCSF Chimera: A visualization system for exploratory research and analysis. *J. Comput. Chem.* **25**, 1605–1612.

- (24) Hall, R. S., Xiang, D. F., Xu, C., and Raushel, F. M. (2007) N-Acetyl-D-glucosamine-6-phosphate deacetylase: Substrate activation via a single divalent metal ion. *Biochemistry* 46, 7942–7952.
- (25) Kamat, S. S., Bagaria, A., Kumaran, D., Hampton, G. P., Fan, H., Sali, A., Sauder, J. M., Burley, S. K., Lindahl, P. A., Swaminathan, S., and Raushel, F. M. (2011) Catalytic mechanism and three-dimensional structure of adenine deaminase. *Biochemistry* 50, 1917–1927.
- (26) Xiang, D. F., Kolb, P., Fedorov, A. A., Meier, M. M., Fedorov, L. V., Nguyen, T. T., Sterner, R., Almo, S. C., Shoichet, B. K., and Raushel, F. M. (2009) Functional annotation and three-dimensional structure of Dr0930 from *Deinococcus radiodurans*, a close relative of phosphotriesterase in the amidohydrolase superfamily. *Biochemistry* 48, 2237–2247.